New nitrogen-rich azo-bridged porphyrin conjugated microporous networks for high performance of gas capture and storage

By: Yanfei Xu, Zhi Li, Fan Zhang, Xiaodong Zhuang, Zheng Zeng, and Jianjun Wei

Y. Xu, Z. Li, F. Zhang, X. Zhuang, Z. Zeng, J. Wei, New nitrogen-rich azo-bridged porphyrin conjugated microporous networks for high performance of gas capture and storage, *RSC Advances*, **2016**, 6 (36), 30048-30055, http://www.doi.org/10.1039/C6RA04077B

Abstract:

A series of new conjugated microporous polymers (Azo-1, Azo-2 and Azo-3) based on a nitrogen-rich porphyrin building unit and an azo bond linkage were synthesized by KOH assisted condensation. These materials were characterized by Fourier transform infrared spectroscopy (FT-IR), solid-state ^{13}C NMR, XPS, scanning electron microscopy (SEM), high-resolution transmission electron microscopy (TEM), X-ray diffraction (XRD), thermogravimetric analysis (TGA), and tested for gas (N_2, CO_2 and H_2) adsorption. It was revealed that the azos presented the formation of porous polymer networks affording amorphous particles with rough surfaces and irregular morphology with excellent thermal stability under nitrogen conditions. The Brunauer–Emmett–Teller (BET) model of the N_2 adsorption gave apparent surface area ranges of 520–675 $m^2\ g^{-1}$. The results from non-local density functional theory (NL-DFT) calculations suggested a pore size distribution between 1.6 and 4.0 nm. The gas (CO_2, H_2) adsorption isotherms demonstrated outstanding CO_2 uptake up to 17.5 wt% (3.98 mmol g^{-1} for Azo-2) and moderate H_2 storage. The isosteric heats of adsorption (Q_{st}) are high, with values of 36–37 kJ mol^{-1} for the azo polymers. Moreover, the azo-polymer networks exhibited excellent selectivity with CO_2/N_2 up to 64.3 for Azo-2 at 273 K/1 bar. It was suggested that the nitrogen-rich active sites of the polymers play an important role for CO_2 capture and storage.

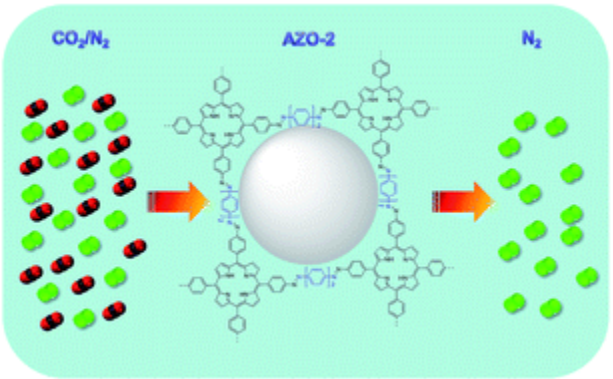

Keywords: conjugated microporous polymers | azo polymers | carbon capture

Article:

Introduction

Porous polymers[1–3] generally possess permanent porosity, low mass densities, synthetic diversification, and high physicochemical stability, which make them highly competitive in gas capture, storage and separation applications.[4–6] Especially for H_2 storage[7–9] and CO_2 storage and separation,[10–12] porous polymers are considered as promising materials. Increasing CO_2 concentration in the atmosphere mainly caused by the rapid consumption of fossil fuels[13] has partly led to the global climate change and some environmental issues,[14] which have drawn great attentions and concerns. Consequently, CO_2 capture and storage is of great interest to meet the energy and environmental demands.

In order to enhance the adsorption interactions and selectivity of CO_2 capture, nitrogen has been doped into many porous materials, such as carbon-based materials,[15–19] microporous polymer networks.[20] Great efforts have been taken to introduce functional amines into the carbon networks *via* organic grafting or direct heat treatment, however, these technologies by post-introduction of amines suffer from some drawbacks of time consuming, high-temperature need, and/or high cost. Recently, N-rich porous polymer networks demonstrate excellence in CO_2 caption and conversion. Coskun group[21] reported a nanoporous polymers incorporating N-heterocyclic carbenes for CO_2 capture and conversion. The resulting polymer networks possess a Brunauer–Emmett–Teller (BET) surface area of 475 $m^2\ g^{-1}$ and CO_2 uptake of ~9.55 wt% (2.1 mmol g^{-1}) at 298 K/1 bar.

Conjugated micro- and mesoporous polymers (CMPs) that permit the linking of building blocks in a π-conjugated fashion are a class of porous materials with 3D or 2D networks and high surface areas,[22] which have attracted much attention. CMPs is an interesting platform for the molecular design of porous skeletons because they allow to manipulate their networks and to tune the porous parameters. One of the remarkable characteristics of CMPs is their crosslinked 3D molecular skeletons.[23] These structural features provide capability of mass transport of the gases into the strictly microporous insides.

Up to date, one of the most characteristic features of CMPs is the rather broad diversity of π-units.[22] Molecular building blocks, ranging from simple phenyl units to extended arenes, heterocyclic aromatic units and large macrocycles, have been successfully exploited for the synthesis of porous polymers. Recently, porphyrin and its derivatives have become one of the major building blocks[24–26] for porous polymer because they possess large planar π-conjugated structure, peculiar electronic properties, good photochemical effect, thermal stability,[27,28] and so on. Liu, *et al.*[29] reported a class of metal functional microporous covalent triazine network prepared using a metalloporphyrin for enhanced CO_2 uptake. It presented a very high BET specific area up to ~1500 $m^2\ g^{-1}$, and excellent CO_2 uptake capability of 3.17 mmol g^{-1}, (13.9 wt%). More recently, a porphyrin polymer with benzimidazole linkages[30] was synthesized to form a rigid amorphous network that exhibited selective CO_2 adsorption with capability of 12.1 wt% (2.76 mmol g^{-1}) and a CO_2/N_2 selectivity of 72 at 273 K/1 bar operation, evident the nanoporous porphyrin networks for gas capture and storage.

Furthermore, some azo-bridged porous polymers have been developed for CO_2 capturing properties. Azo-linked porous organic framework (a 2D layered Azo-POF-2) exhibited high CO_2/N_2 selectivity of 76 at 273 K.[31] Arab *et al.* reported[32] a series of new azo-linked polymers (ALPs), with surface area of 412–801 $m^2\ g^{-1}$, demonstrated CO_2 uptake capacities of up to 2.94 mmol g^{-1} at 298 K/1 bar and good CO_2/N_2 selectivity (56). Another class of ALPs, synthesized by homocoupling of aniline-like building units in the presence of copper(i) bromide and pyridine, possessing higher surface area of 862–1235 $m^2\ g^{-1}$, presented higher CO_2 uptake capacities of up to 5.37 mmol g^{-1} at 237 K/1 bar.[33] The investigation shows that the porosity parameters (surface area, pore volume and pore size) play key roles in CO_2 uptake capacity and CO_2 selectivity.

In this paper, combining the advantages of CMPs with the porphyrin units, a series of unprecedented, electron-rich conjugated microporous polymers (Azo-1, Azo-2, and Azo-3) based on nitrogen-rich porphyrin building units and azo bond linkage was synthesized by KOH assisted condensation. The azo-polymer networks were characterized by solid-state NMR spectroscopy, infrared spectroscopy, and elemental analysis to obtain their structural and chemical composition. Thermogravimetric analysis showed that all azos networks exhibit a high thermal stability under N_2. Despite their moderate specific BET equivalent surface areas (520–675 $m^2\ g^{-1}$), they featured remarkable CO_2 uptakes up to 17.52 wt% (3.98 mmol g^{-1}) and excellent selectivity (CO_2/N_2 ratio 15/1) at 273 K/1 bar, and moderate capability for H_2 storage (1.15 wt%, 5.75 mmol g^{-1}) at 77 K/1 bar. High CO_2 adsorption is expected to occur because of the Lewis acid–base interactions between the active electron-rich aromatic constituents and the electron-poor CO_2 molecules.

Experimental

Materials

Pyridine (99.5%), acetic anhydride (98.5%), potassium hydroxide (90%), and propionic acid (99%) were purchased from Sinopharm Chemical Reagent Co. Ltd. *p*-Nitrobenzaldehyde (99%) was obtained from Adamas. *p*-Phenylenediamine (99%) was purchased from Sigma-Aldrich. Melamine (99%) and *N*,*N*-dimethylformamide (DMF) (99.8%) were obtained from J&K Chemical. Pyrrole (99%) and benzidine (98%) were purchased from Energy Chemical. Pyrrole was freshly distilled before used, and the other chemicals were used as received.

Synthetic procedures

Synthesis of 5,10,15,20-tetrakis(4-nitrophenyl)-21*H*,23*H*-porphine (TNPP). TNNP synthesis was followed the experimental procedure in literature.[34] *p*-Nitrobenzaldehyde (22.0 g, 145 mmol) and acetic anhydride (24.0 mL, 254 mmol) were dissolved in propionic acid (600 mL). The solution was then refluxed, to which freshly distilled pyrrole (10.0 mL, 144 mmol) was slowly added. After refluxing for 30 min, the resulting mixture was cooled to the room temperature. Then the precipitate was collected by filtration, washed with distilled water and methanol, and dried under vacuum. The resulting powder was dissolved in pyridine (160 mL) which was refluxed for 1 h. After cooling, the precipitate was collected by filtration and washed with acetone to give 4.5 g TNPP as a purple crystal in 15.6% yield. Elem. anal. calcd for

$C_{44}H_{26}N_8O_8$ (%): C, 66.50; N, 16.11. Found: C, 65.62; N, 13.38. HRMS (EI-MS): $C_{44}H_{26}N_8O_8$ for $[M + H]^+$, calculated 795.1874; found 795.1947.

Synthesis of Azo-1. TNPP (0.3176 g, 0.4 mmol), *p*-phenylenediamine (0.0865 g, 0.8 mmol) and KOH (0.22 g, 3.94 mmol) were dissolved in DMF (25 mL). The reaction mixture was heated to 150 °C and stirred for 24 h under a nitrogen atmosphere. The reaction mixture was cooled down to room temperature, added with 150 mL of distilled water and stirred for 1 h. Black precipitate was filtered off and washed several times with distilled water, acetone and THF in order to remove any unreacted monomers and KOH. Subsequently, black precipitates were dried at 60 °C under vacuum overnight to yield Azo-1: 0.26 g. Yield was 64% with elemental analysis of C: 72.08; H: 4.50; N: 14.92 (%).

Synthesis of Azo-2 and Azo-3. The procedure is similar to the synthetic route of Azo-1. The details of the procedure and product data are provided in ESI.†

Characterization methods and testing of gas sorption

Characterization methods. Fourier transform infrared spectroscopy (FT-IR) was performed on a Spectrum 100 (Perkin Elmer, Inc., USA) spectrometer with a scan range of 4000–400 cm^{-1}. The sample powders were pulverized with KBr, and pressed into disks. Solid-state ^{13}C cross polarization/magic angle spinning nuclear magnetic resonance (CP/MAS NMR) analysis was conducted on a Bruker AVANCE III 300 Spectrometer. Meanwhile, the cross polarization/magic angle spinning nuclear magnetic resonance (CP/MAS NMR) experiments were achieved by incorporating the total side-band suppression (TOSS) pulse. Samples were spun at 5 kHz in 4 mm rotor within a MAS probe. An acquisition time of 20 ms, a contact time of 1 ms and a 6.5 μs pre-scan delay were used. The recycle time was 2 s to obtain fully relaxed spectra. Chemical shifts were externally referenced to adamantane at 38.48 ppm. X-ray photoelectron spectroscopy (XPS) was performed using an AXIS Ultra DLD system (Kratos Co., Japan) with Al Kα radiation as the X-ray source. Thermogravimetric analysis (TGA) of the samples was undertaken using a Q5000IR (TA Instruments, USA) thermogravimetric analyzer with a heating rate of 20 °C min^{-1} from room temperature up to 800 °C under nitrogen flow. Scanning electron microscopy (SEM) was performed using an FEI Sirion-200 (FEI Co., USA) field emission scanning electron microscope. Transmission electron microscopy (TEM) observations were carried out with a JEOL-2100 (JEOL Ltd., Japan) electron microscope at an operating voltage of 200 kV. X-ray diffraction (XRD) measurements were performed using a Rigaku D/Max 2500 X-ray diffractometer with Cu Kα radiation (k = 1.54 Å) at a generator voltage of 40 kV and a generator current of 50 mA with a scanning speed of 2° min^{-1} from 2° to 35°. HRMS was performed on Q-Tof Premier (Waters, USA).

Testing of gas sorption. The gas sorption isotherms were measured *via* an Autosorb-iQA3200-4 (ASIQA3200-4) sorption analyzer (Quantatech Co., USA). Nitrogen adsorption/desorption isotherms were measured at 77 K using a Quantachrome ASIQA3200-4 gas sorption analyser. Carbon dioxide (CO_2) measurements were measured at 273 and 298 K using a Quantachrome ASIQA3200-4 extended sorption analyser fitted with a chiller circulator dewar. Hydrogen (H_2) sorption isotherm measurements were analyzer at 77 and 87 K. Prior to the measurement, the samples were degassed in vacuum 150 °C for 4 h. The isosteric heats of adsorption were

calculated using the standard calculation routines provided with the ASIQA3200-4 software. The pore size distribution was calculated from non-local density functional theory (NL-DFT).

Results and discussion

Synthesis

The strategy for the synthesis of azo-bridged porphyrin-based conjugated microporous polymers (Azo-1, Azo-2, and Azo-3) is presented in Scheme 1S.† From previous report,[35] azo compounds can be prepared by simple synthetic protocols. However, we choose azo condensation reaction to connect the building blocks and synthesis of conjugated polymers for the following reasons: (1) azo condensation is an efficient, well-established process and does not require expensive catalysts; (2) it can introduce azo bonds into the conjugated structure that can produce electron-rich conjugated networks; (3) it promotes the binding between the electron-rich azo series and the electron-poorer CO_2.

Structural and chemical characterization

FT-IR spectra of Azo-1, Azo-2, and Azo-3 show the characteristic –N=N– stretching band at around 1598, 1597 and 1598 cm^{-1} ($\lambda_{N=N}$: 1630–1580 cm^{-1})[36] along with the respective bands for aromatic rings (see Fig. 1), which is not appearing in the building block TNPP. Furthermore, several weak bands are observed in the region from 1300 to 1520 cm^{-1}. Compared with the bands located in TNPP, the bands of azo series are much weaker, indicating that the degree of polymerization is high. The bands located at 1510 and 1344 cm^{-1} correspond to N–O stretching mode,[35] suggesting most terminal nitro groups were reacted.

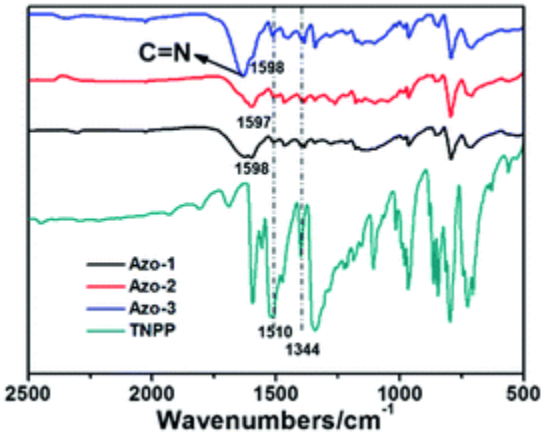

Fig. 1 FT-IR spectra of Azo-1, Azo-2, Azo-3, and TNPP.

In the solid-state ^{13}C CP/MAS NMR spectra (Fig. 2), Azo-1, Azo-2, and Azo-3 gave signals of chemical shift at 151.6, 144.2, 131.2, and 118.1 ppm, which were consistent with those of azo-linked aromatic polymers,[37] attributing to the carbon atoms of the porphyrin rings and phenyl linkers.[38,39] The carbons bonded to the azine nitrogen (–N=C–) appear at 151.6 ppm whereas those bonded to the imino nitrogen (–NH–) appear at 118.1 ppm, suggesting that the downfield carbon resonance should be assigned to the α-pyrrolenine-like ring and the high-field resonance

to the (1*H*)-pyrrole-like ring.[40] As expected, a typical peak at around 151.6 ppm, attributed to the azo-linked aromatic carbons (–C_{ar}–N=N–C_{ar}–),[41] is found for Azo-1, Azo-2, and Azo-3.

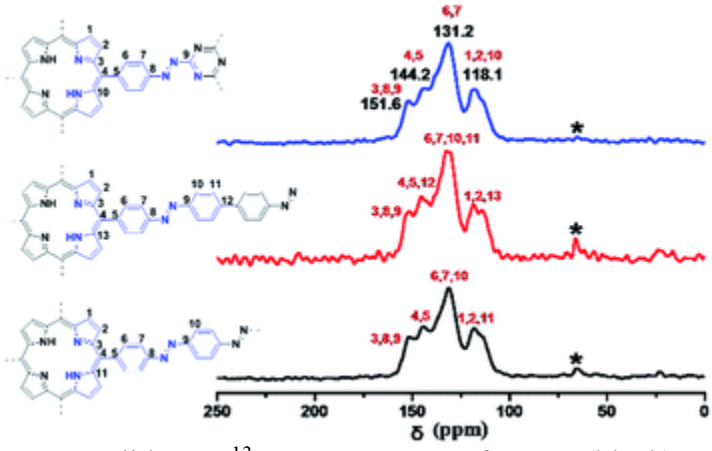

Fig. 2 Solid-state ^{13}C NMR spectra of Azo-1 (black), Azo-3 (red) and Azo-3 (blue). Asterisks represent spinning sidebands.

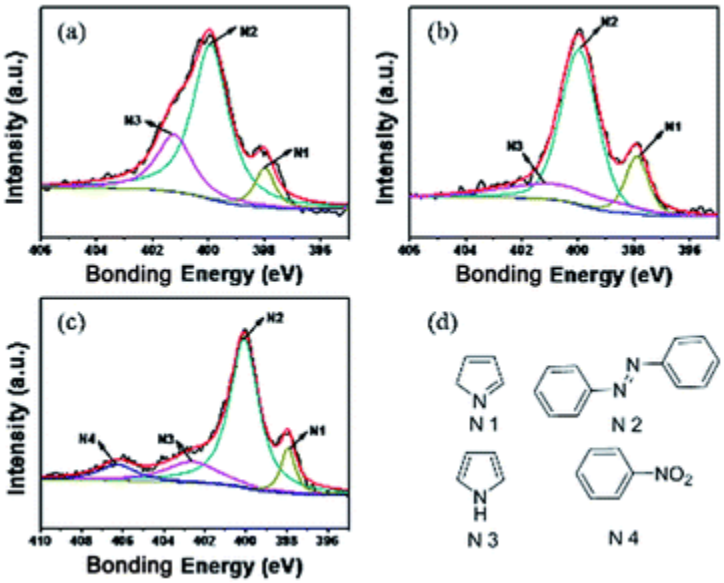

Fig. 3 N 1s XPS spectra (a–c) and different nitrogen species for azos (a: Azo-1, b: Azo-2, c: Azo-3), and (d) different structures containing nitrogen (N1–4).

XPS was performed to analyze the elemental composition and nitrogen bonding configurations in azo series. The XPS survey spectrum shows the presence of carbon, nitrogen, and oxygen distinctly compared with the theoretical vales of 850 eV, 399 eV, and 533 eV,[42] respectively (see Fig. S1†). The bonding configurations of nitrogen in azos are revealed by the N 1s core level spectra (Fig. 3a–c). All of the nitrogen responses of Azo-1 and Azo-2, giving 398.0, 399.9, and 401.0 eV, correspond to the imine nitrogen[43] (–C=N–) (N1), azo nitrogen (Ph–N=N–Ph) (N2), and pyrrolic nitrogen (–NH–) (N3), respectively.[44,45] The nitrogen responses of Azo-3 can be deconvoluted into five types: 398.0, 399.9, 401.0, and 405.7, corresponding to the imine nitrogen (–C=N–) (N1), azo nitrogen (Ph–N=N–Ph) (N2), pyrrolic nitrogen (–NH–) (N3), and nitro nitrogen (Ph–NO_2) (N4), respectively (Fig. 3d). The integral areas of these five peaks for azos

were used to calculate the content of nitrogen species (N1–N4, Fig. S1†), from which we can find the ratio of N4 for Azo-3 is the highest, suggesting that the degree of polymerization is lower than the other two polymer networks.

TGA was performed on Azo-1, Azo-2, and Azo-3 to determine the thermal stability and to confirm the absence of guest molecules inside the pores (see Fig. S2†). Azo-1 shows mass loss around 0.30% at temperature 132 °C, which is possibly caused by loss of volatiles (such as moisture) or trapped solvent molecules in the polymer networks when compared to that of TNPP. Similarly, Azo-2 shows mass loss around 2.41% at temperature 100 °C, and Azo-3 shows mass loss around 0.99% at 133 °C. Due to the decomposition of the network, a gradual weight loss of 5% for Azo-1, Azo-2, Azo-3 was observed after 317 °C, 135 °C, 305 °C, respectively and about 10% weight loss at 500 °C for all. Overall, Azo-1, Azo-2, and Azo-3 retain 65.63%, 68.05%, 66.97% of their mass respectively at 800 °C as revealed by TGA experiments, similar to that of TNNP. However, azo series presents less weight loss between 400 and 500 °C, which may be ascribable to the high degree of polymerization. These results highlight that Azo-1/2/3 have excellent thermal stability in a nitrogen atmosphere.

Morphological and crystallographic characterization

The morphology and microstructure of the Azo-1, Azo-2, and Azo-3 were investigated by SEM and TEM. All of the polymer networks illustrated similar morphology; Fig. 4 shows the representative SEM and TEM images of Azo-1 (more see Fig. S3†). Similar to other microporous polymers,[46,47]Fig. 4a shows the azo polymer networks are wrinkles, and composing of loose agglomerates of tiny particles with rough surface and irregular shapes. For the sake of clarity, an enlarged TEM images are presented in Fig. 4b. The white region corresponds to the nanopore channels, while the dark region is attributed to the polymer networks skeleton. It clearly shows that the pores in the polymer networks are quite uniform and the polymer networks demonstrate typical microporous materials.

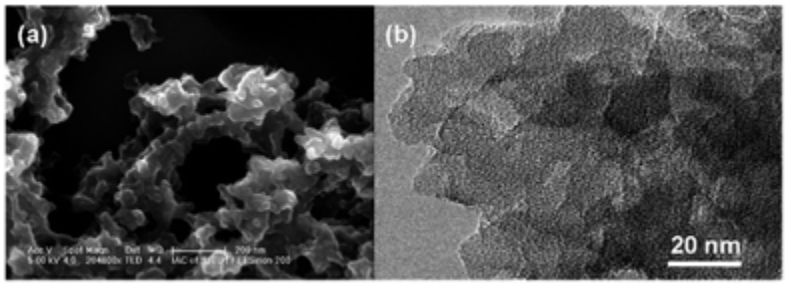

Fig. 4 A typical (a) SEM image and (b) TEM image of Azo-1 polymer.

In order to elucidate the crystallinity of the azo series, these polymer networks were also characterized by XRD (see Fig. S4†), intense peaks in the XRD patterns of Azo-1, Azo-2 and Azo-3 were not found except some minor peaks, indicating that Azo-1, Azo-2 and Azo-3 are mostly amorphous, which was consistent with previous SEM and TEM images showing litter crystallinity within the polymer networks. Indeed, conjugated microporous polymers are known to be amorphous solids.[14]

Studies of gas sorption and storage

Gas sorption. The permanent porosity in the networks was investigated by sorption analysis using N_2, CO_2, and H_2 as the adsorbate molecules. Fig. 5a shows the N_2 adsorption and desorption isotherms for Azo-1/2/3, while Table 1 summarizes the porous properties of a few comparable polymer networks. Azo-1, Azo-2, and Azo-3 displayed type II isotherms with type I character at higher relative pressures according to IUPAC classification. In Fig. 5a, one can find all of the desorption isotherms of the three networks exhibit some extent hysteresis, suggesting the presence of some mesoporous within the materials. The calculated Brunauer–Emmett–Teller (BET) specific surface areas of the azo series are 571 $m^2 g^{-1}$, 675 $m^2 g^{-1}$, and 520 $m^2 g^{-1}$, and the Langmuir surface areas 668 $m^2 g^{-1}$, 730 $m^2 g^{-1}$, and 610 $m^2 g^{-1}$ for Azo-1, Azo-2, and Azo-3, respectively. From the robust porous features of the three materials presented in Table 1, we found that total pore volumes of the azo series are 1.342 $cm^3 g^{-1}$, 1.686 $cm^3 g^{-1}$, 1.383 $cm^3 g^{-1}$ for Azo-1, Azo-2, and Azo-3, respectively. These values are comparable or higher than that of previously reported microporous materials constructed through azo condensation.[37]

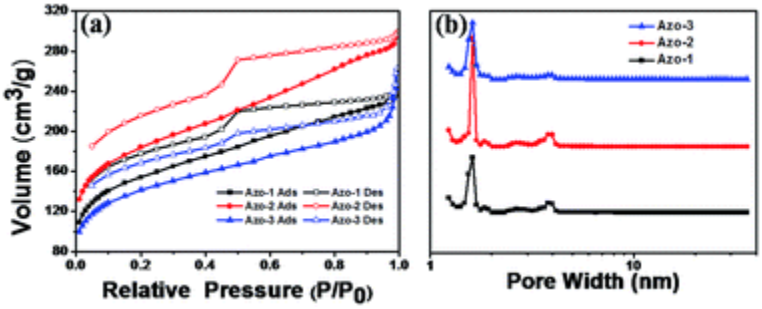

Fig. 5 (a) N_2 adsorption (solid) and desorption (hollow) isotherms of Azo-1, Azo-2 and Azo-3 at 77 K; (b) pore size distribution of azo series.

Table 1. Surface properties and gas uptake for Azo-1/2/3

Polymer network	S_{BET} [$m^2 g^{-1}$]	$S_{Langmuir}$ [$m^2 g^{-1}$]	d_{AV}[a] [nm]	S_{MICRO} [$m^2 g^{-1}$]	V_{MICRO} [$cm^3 g^{-1}$]	V_{TOT}[b] [$cm^3 g^{-1}$]	V_{MICRO}/V_{TOT}	H_2 uptake [wt%] 77 K	H_2 uptake [wt%] 87 K	CO_2 uptake [wt%] 273 K	CO_2 uptake [wt%] 298 K
Azo-1	571	668	3.47	338	0.156	1.342	0.12	0.86	0.76	9.42	7.11
Azo-2	675	730	2.72	437	0.186	1.686	0.11	1.15	0.80	17.52	8.97
Azo-3	520	610	2.89	376	0.164	1.383	0.12	0.97	0.71	12.63	6.60

[a] Note: average pore diameter. [b] Note: total pore volume at $P/P^0 = 0.99$.

Fig. 5b shows the pore size distribution (PSD) curves for the three polymer networks as calculated using NL-DFT. Azo-1 exhibits average pore diameter centering at around 3.47 nm with a major peak at 1.6 nm, and a minor peak in the 3.8–4.0 nm region. Azo-2 presents average pore diameter centering at around 2.72 nm with a major peak at 1.6 nm, and a minor in the 3.8–4.0 nm region. Azo-3 gives average pore diameter centering at around 2.89 nm with a major peak at 1.6 nm, and a minor in the 3.8–4.0 nm region. In addition, all of the networks show weak peaks in the size range of 2–4 nm. The PSD analysis agrees with the results of the N_2 isotherms (Fig. 5a), suggesting that the azo polymers feature some mesopores within the micropore structures. Since types I isotherm corresponds to microporous materials, and type IV is attributed for mesoporous materials. So the nitrogen isotherms of azos show type I with type IV character.[48] The contribution of microporosity to the networks can be calculated as the ratio of the micropore volume, V_{MICRO}, over the total pore volume, V_{TOTAL}. The ratios indicate networks Azo-1/2/3 possess a similar ratio of 0.11–0.12. The results along with TEM images indicate that

Azo-1/2/3 are typical microporous materials. The ratio of Azo-2 is similar to that of Azo-1/3, but the absolute micropore volume per g of Azo-2 is larger than that of Azo-1/3, which may explain its higher N_2 adsorption, and the higher BET specific surface area.

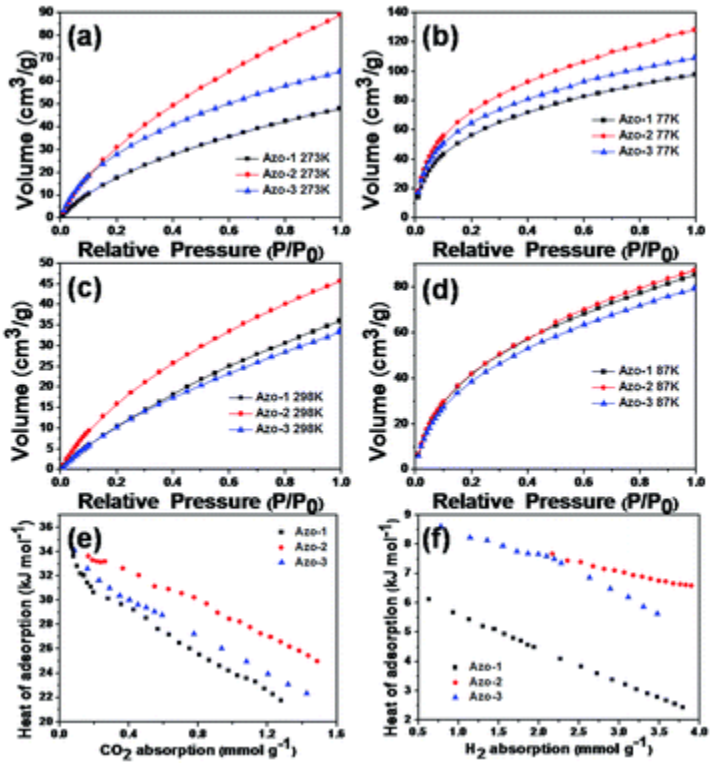

Fig. 6 Gas adsorption studies. (a) CO_2 adsorption isotherms of Azo-1, Azo-2, and Azo-3 at 273 K (a) and 298 K (c). H_2 adsorption isotherms of Azo-1, Azo-2, and Azo-3 at 77 K (b) and 87 K (d). Isosteric heats of adsorption of Azo-1, Azo-2, and Azo-3 for CO_2 (e) and H_2 (f).

The large surface area, microporous structure and narrow pore size distribution of the polymer networks and nitrogen-enriched networks intrigue us to further explore their application in CO_2 capture and separation from other gases. The CO_2 sorption of the polymer networks were investigated by a volumetric method at 273 and 298 K (Fig. 6). For all the three polymers, the CO_2 uptake appears a rapid rise in the initial stage, implying that CO_2 molecule has favorable interaction with the polymer skeleton. Moreover, it is noted that the uptake of CO_2 continually increases with the relative pressure in the experimental range, suggesting that a higher adsorption capacity can be achieved at the high pressure. Fig. 6a shows the CO_2 uptakes by Azo-1/2/3 are 94.2 mg g^{-1}, 175.2 mg g^{-1}, and 126.3 mg g^{-1} at 273 K and 1 bar, respectively. Azo-2 obtains the highest CO_2 uptake (3.98 mmol g^{-1}, 17.52 wt% at 273 K/1 bar), which may be ascribed to its larger micropore volume as shown in previous BET values. Additionally, it was found that Azo-3 exhibits a higher CO_2 adsorption capacity than Azo-1 even though its apparent BET surface area is lower. This difference may arise from pore size distribution effect of azo and the difference in micropore volume (V_{MICRO} for Azo-1, Azo-3 is 0.156, 0.164 cm^3 g^{-1}, respectively). It has been reported that the micropore volume has a stronger effect on the gas uptakes of a material than the total pore volume and the specific surface area.[49] On the other hand, it is expected that the CO_2 uptake of the azo networks decrease at 298 K (which are 71.1 mg g^{-1} for

Azo-1, 89.7 mg g^{-1} for Azo-2, and 66.0 mg g^{-1} for Azo-3, see Fig. 5c). These values are still comparable to or better than that of very high surface area porous polymers (Table S1 in ESI†).

We have further studied the hydrogen (H_2) sorption performance of the azo series in powder form. The H_2 sorption of the network polymers were investigated by the volumetric method at 77 and 88 K. Fig. 6b and d shows the H_2 adsorption isotherms up to a maximum H_2 pressure of 1 bar. At 77 K, the H_2 uptakes are 8.6 mg g^{-1} for Azo-1, 11.5 mg g^{-1} for Azo-2, and 9.7 mg g^{-1} for Azo-3 (Fig. 6b). Azo-2 exhibits the largest H_2 uptake of 5.75 mmol g^{-1} at 77 K/1 bar (1.15 wt%). Uptakes of H_2 are in the order of Azo-2 > Azo-3 > Azo-1, as same as the order of CO_2 sorption of these networks. This can also be explained by the pore size distribution effects and the difference in micropore volume. As expected, the H_2 uptakes of networks decrease at 87 K to 7.6 mg g^{-1} for Azo-1, 8.0 mg g^{-1} for Azo-2, and 7.1 mg g^{-1} for Azo-3 (Fig. 6d). Compared to the reported porous networks (Table S2 in ESI†), the capability of H_2 uptakes is moderate.

Heats of adsorption. To further understand the pore surface characteristics of the materials and the adsorption process, the isosteric heats of adsorption (Q_{st}) for CO_2 and H_2 were investigated. Q_{st} of CO_2 was calculated using the Clausius–Clapeyron equation from the sorption data collected at 273 and 298 K. Fig. 6e shows Q_{st} of CO_2 for Azo-1/2/3. At the adsorption onset, the Q_{st} values for Azo-1, Azo-2 and Azo-3 are 37, 36, and 36 kJ mol^{-1}, respectively. The values are higher than that of other porous materials, such as high surface area MPIs (30.4–34.8 kJ mol^{-1}),[50] electron-rich PECONFs (29–34 kJ mol^{-1}),[51] imine-linked PPFs (21.8–29.2 kJ mol^{-1}),[52] and comparable to or higher than microporous polymers with organic ammonium ions or Lewis basic amine in pores (30–55 kJ mol^{-1}).[53,54] The heat of adsorption drops by 40% (Azo-1), 30.1% (Azo-2) and 37.5% (Azo-3) during the CO_2 uptake experiments, suggesting that, if the pore volumes of the materials can be further increased, a significantly enhanced CO_2 gas uptake can probably be achieved even at low CO_2 pressure. The Clausius–Clapeyron equation for heat adsorption is given as below:[55]

$$\ln P = \frac{Q_{st}}{RT} + C \qquad (1)$$

where P, T, R and C are the pressure, temperature at the equilibrium state, the gas constant, and equation constant, respectively.

From the sorption data collected at 77 and 87 K, Q_{st} of H_2 adsorption was calculated using the eqn (1) too. Fig. 6f shows Q_{st} of Azo-1, Azo-2 and Azo-3 are of 6.2, 8.5 and 8.8 kJ mol^{-1} respectively at the adsorption onset. The heat of adsorption decreases slightly with increased hydrogen loading. Compared to the isosteric heats of adsorption for CO_2, adsorption of H_2 at the surfaces of the azo networks is much less, mainly because of little active sites at the surfaces of the materials. Physisorption of the H_2 contributes the most for its adsorption.

Gas selectivity. To assess the potential applications of these networks in post combustion CO_2 capture under ambient pressure, single component gas adsorption isotherms were carried out with CO_2 or N_2 under 273 K and up to 1 bar (Fig. 7). The selectivity for CO_2 over N_2 was calculated by the ratios of the initial slopes of CO_2 and N_2 adsorption isotherms based on the pressure below 0.10 bar and the ideal adsorbed solution theory.[56] Azo-1, Azo-2 and Azo-3 give CO_2/N_2 selectivity of 42.1, 64.3 and 44.5, respectively, based on the initial 5 data points (<0.1

bar) of the isotherm curves, indicating greatly increased selectivity of Azo-2 for CO_2 uptake over N_2. The high CO_2 adsorption capacity and CO_2/N_2 adsorption selectivity are the two key parameters for evaluating the potential of porous materials in carbon dioxide capture applications. The excellent selective adsorption of CO_2 may pave the way to CO_2 capture and separation, as well as air-cleaning applications by the microporous materials.

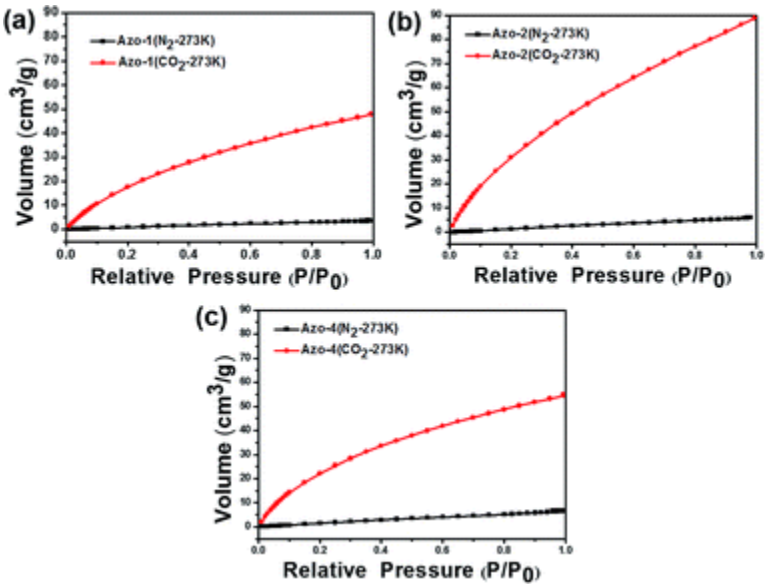

Fig. 7 Adsorption isotherms of CO_2 and N_2 gases at 273 K for Azo-1 (a), Azo-2 (b), and Azo-3 (c).

Conclusions

A series of new conjugated microporous polymers, Azo-1, Azo-2, and Azo-3 was successfully synthesized through azo condensation of TNPP with *p*-phenylenediamine, benzidine and melamine, respectively. Their chemical structures were confirmed by FT-IR and solid-state ^{13}C CP/MAS NMR measurements. TGA measurements showed excellent thermal stability of these networks. XRD studies indicated amorphous structure of the polymers. Pore size distributions revealed a mainly microporous network structure for Azo-1, Azo-2, and Azo-3 with BET surface areas of 571 $m^2\ g^{-1}$, 675 $m^2\ g^{-1}$, and 520 $m^2\ g^{-1}$, respectively, whereas Azo-2 distinguishes by its higher micropore volume. Under the present reaction conditions, pore sizes between 1.6 and 4 nm were obtained. Owing to the narrow pore size distribution and nitrogen-rich pore surfaces, azo series exhibit exceptionally high CO_2 uptake. Thanks to the bigger nano-micropore volume, Azo-2 showed the highest BET surface area up to 675 $m^2\ g^{-1}$ and a remarkable CO_2 uptake of 3.98 mmol g^{-1} (or 17.52 wt%) at 273 K and 1 bar pressure. The heat of adsorption for CO_2 was calculated to be 36–37 kJ mol^{-1}, which is larger than that of many reported porous materials. Moreover, azos showed excellent adsorption selectivity with CO_2/N_2 up to 64.3 for Azo-2 at 273 K/1 bar. The H_2 storage capability of the Azo-1/2/3 is moderate through physisorption of the azo polymers. The above results indicate that the reported azo porous polymer networks are promising candidates as adsorbents for CO_2 capture, separation and storage, and will be exploited for CO_2 caption in industrial (*e.g.* combustion gas) and environmental air-cleaning.

Acknowledgements

The authors thank the financial support from National Natural Science Foundation of China (51403126). ZZ and JW acknowledge the support from the JSNN at UNCG.

Footnote

† Electronic supplementary information (ESI) available: Additional experimental data for materials. See DOI: 10.1039/c6ra04077b

Notes and references

1. A. Thomas , P. Kuhn , J. Weber , M. M. Titirici and M. Antonietti , *Macromol. Rapid Commun.*, 2009, **30** , 221 —236.
2. D. Wu , F. Xu , B. Sun , R. Fu , H. He and K. Matyjaszewski , *Chem. Rev.*, 2012, **112** , 3959 —4015.
3. Z. Xiang and D. Cao , *J. Mater. Chem. A*, 2013, **1** , 2691 —2718.
4. Q. Chen , M. Luo , P. Hammershøj , D. Zhou , Y. Han , B. W. Laursen , C.-G. Yan and B.-H. Han , *J. Am. Chem. Soc.*, 2012, **134** , 6084 —6087.
5. D. Yuan , W. Lu , D. Zhao and H. C. Zhou , *Adv. Mater.*, 2011, **23** , 3723 —3725.
6. W. Lu , D. Yuan , J. Sculley , D. Zhao , R. Krishna and H.-C. Zhou , *J. Am. Chem. Soc.*, 2011, **133** , 18126 —18129.
7. J. Germain , J. M. Fréchet and F. Svec , *Small*, 2009, **5** , 1098 —1111.
8. O. K. Farha , A. Ö. Yazaydın , I. Eryazici , C. D. Malliakas , B. G. Hauser , M. G. Kanatzidis , S. T. Nguyen , R. Q. Snurr and J. T. Hupp , *Nat. Chem.*, 2010, **2** , 944 —948.
9. M. Pumera *Energy Environ. Sci.*, 2011, **4** , 668 —674.
10. D. M. D'Alessandro , B. Smit and J. R. Long , *Angew. Chem., Int. Ed.*, 2010, **49** , 6058 — 6082.
11. G. Férey , C. Serre , T. Devic , G. Maurin , H. Jobic , P. L. Llewellyn , G. De Weireld , A. Vimont , M. Daturi and J.-S. Chang , *Chem. Soc. Rev.*, 2011, **40** , 550 —562.
12. R. Dawson , E. Stöckel , J. R. Holst , D. J. Adams and A. I. Cooper , *Energy Environ. Sci.*, 2011, **4** , 4239 —4245.
13. N. Du , H. B. Park , G. P. Robertson , M. M. Dal-Cin , T. Visser , L. Scoles and M. D. Guiver , *Nat. Mater.*, 2011, **10** , 372 —375.
14. N. B. McKeown and P. M. Budd , *Chem. Soc. Rev.*, 2006, **35** , 675 —683.
15. J. Wang , I. Senkovska , M. Oschatz , M. R. Lohe , L. Borchardt , A. Heerwig , Q. Liu and S. Kaskel , *ACS Appl. Mater. Interfaces*, 2013, **5** , 3160 —3167.
16. G. Sethia and A. Sayari , *Carbon*, 2015, **93** , 68 —80.

17. G.-P. Hao , W.-C. Li , D. Qian and A.-H. Lu , *Adv. Mater.*, 2010, **22** , 853 —857.

18. K. Huang , S.-H. Chai , R. T. Mayes , G. M. Veith , K. L. Browning , M. A. Sakwa-Novak , M. E. Potter , C. W. Jones , Y.-T. Wu and S. Dai , *Chem. Commun.*, 2015, **51** , 17261 —17264.

19. G. Sethia and A. Sayari , *Energy Fuels*, 2014, **28** , 2727 —2731.

20. N. Popp , T. Homburg , N. Stock and J. Senker , *J. Mater. Chem. A*, 2015, **3** , 18492 —18504.

21. S. N. Talapaneni , O. Buyukcakir , S. H. Je , S. Srinivasan , Y. Seo , K. Polychronopoulou and A. Coskun , *Chem. Mater.*, 2015, **27** , 6818 —6826.

22. Y. Xu , S. Jin , H. Xu , A. Nagai and D. Jiang , *Chem. Soc. Rev.*, 2013, **42** , 7965 —8178.

23. A. I. Cooper *Adv. Mater.*, 2009, **21** , 1291 —1295.

24. Y. Liu , X. Guo , N. Xiang , B. Zhao , H. Huang , H. Li , P. Shen and S. Tan , *J. Mater. Chem.*, 2010, **20** , 1140 —1146.

25. X. Feng , L. Chen , Y. Dong and D. Jiang , *Chem. Commun.*, 2011, **47** , 1979 —1981.

26. N. U. Day , C. C. Wamser and M. G. Walter , *Polym. Int.*, 2015, **64** , 833 —857.

27. W. M. Campbell , K. W. Jolley , P. Wagner , K. Wagner , P. J. Walsh , K. C. Gordon , L. Schmidt-Mende , M. K. Nazeeruddin , Q. Wang and M. Grätzel , *J. Phys. Chem. C*, 2007, **111** , 11760 —11762.

28. W. Zheng , N. Shan , L. Yu and X. Wang , *Dyes Pigm.*, 2008, **77** , 153 —157.

29. X. Liu , H. Li , Y. Zhang , B. Xu , S. A , H. Xia and Y. Mu , *Polym. Chem.*, 2013, **4** , 2445 —2448.

30. V. S. P. K. Neti , J. Wang , S. Deng and L. Echegoyen , *RSC Adv.*, 2015, **5** , 10960 —10963.

31. J. Lu and J. Zhang , *J. Mater. Chem. A*, 2014, **2** , 13831 —13834.

32. P. Arab , E. Parrish , T. Islamoglu and H. M. El-Kaderi , *J. Mater. Chem. A*, 2015, **3** , 20586 —20594.

33. P. Arab , M. G. Rabbani , A. K. Sekizkardes , T. İslamoğlu and H. M. El-Kaderi , *Chem. Mater.*, 2014, **26** , 1385 —1392.

34. M. Yuasa , K. Oyaizu , A. Yamaguchi and M. Kuwakado , *J. Am. Chem. Soc.*, 2004, **126** , 11128 —11129.

35. H. A. Patel , S. Hyun Je , J. Park , D. P. Chen , Y. Jung , C. T. Yavuz and A. Coskun , *Nat. Commun.*, 2013, **4** , 1357.

36. P. Narayanan *Essentials Of Biophysics* , Anshan, 2000.

37. H. A. Patel , S. H. Je , J. Park , D. P. Chen , Y. Jung , C. T. Yavuz and A. Coskun , *Nat. Commun.*, 2013, **4** , 1357.

38. X. Feng , L. Liu , Y. Honsho , A. Saeki , S. Seki , S. Irle , Y. Dong , A. Nagai and D. Jiang , *Angew. Chem.*, 2012, **124** , 2672 —2676.

39. A. Modak , M. Nandi , J. Mondal and A. Bhaumik , *Chem. Commun.*, 2012, **48** , 248 —250.

40. L. Frydman , A. C. Olivieri , L. E. Diaz , A. Valasinas and B. Frydman , *J. Am. Chem. Soc.*, 1988, **110** , 5651 —5661.

41. S. Xie , A. Natansohn and P. Rochon , *Macromolecules*, 1994, **27** , 1489 —1492.

42. A. P. Hitchcock and C. E. Brion , *J. Electron Spectrosc. Relat. Phenom.*, 1980, **18** , 1 —21.

43. A. P. Dementjev , A. de Graaf , M. C. M. van de Sanden , K. I. Maslakov , A. V. Naumkin and A. A. Serov , *Diamond Relat. Mater.*, 2000, **9** , 1904 —1907.

44. L. Silipigni , G. De Luca , Q. Quattrone , L. M. Scolaro , G. Salvato and V. Grasso , *J. Phys.: Condens. Matter*, 2006, **18** , 5759 —5772.

45. W. Lian , Y. Sun , B. Wang , N. Shan and T. Shi , *J. Serb. Chem. Soc.*, 2012, **77** , 335 —348.

46. Y. Yang , Q. Zhang , Z. Zhang and S. Zhang , *J. Mater. Chem. A*, 2013, **1** , 10368 —10374.

47. M. Mastalerz , M. W. Schneider , I. M. Oppel and O. Presly , *Angew. Chem., Int. Ed.*, 2011, **50** , 1046 —1051.

48. G. Crini and P.-M. Badot , *Sorption Processes and Pollution: Conventional and Non-conventional Sorbents for Pollutant Removal from Wastewaters* , Presses Univ. Franche-Comté, 2010.

49. A. P. Katsoulidis and M. G. Kanatzidis , *Chem. Mater.*, 2012, **24** , 471 —479.

50. G. Li and Z. Wang , *Macromolecules*, 2013, **46** , 3058 —3066.

51. P. Mohanty , L. D. Kull and K. Landskron , *Nat. Commun.*, 2011, **2** , 401.

52. Y. Zhu , H. Long and W. Zhang , *Chem. Mater.*, 2013, **25** , 1630 —1635.

53. A. Demessence , D. M. D'Alessandro , M. L. Foo and J. R. Long , *J. Am. Chem. Soc.*, 2009, **131** , 8784 —8786.

54. Y. Fu , D. Sun , Y. Chen , R. Huang , Z. Ding , X. Fu and Z. Li , *Angew. Chem.*, 2012, **124** , 3420 —3423.

55. V. Krungleviciute , L. Heroux , A. D. Migone , C. T. Kingston and B. Simard , *J. Phys. Chem. B*, 2005, **109** , 9317 —9320.

56. X. Zhu , C.-L. Do-Thanh , C. R. Murdock , K. M. Nelson , C. Tian , S. Brown , S. M. Mahurin , D. M. Jenkins , J. Hu , B. Zhao , H. Liu and S. Dai , *ACS Macro Lett.*, 2013, **2** , 660 —663.